Available online at www.sciencedirect.com
ScienceDirect
European Journal of Mechanics B/Fluids 27 (2008) 609–622

Rarefied gas flow in concentric annular tube: Estimation of the Poiseuille number and the exact hydraulic diameter

George Breyiannis, Stelios Varoutis, Dimitris Valougeorgis *

Department of Mechanical and Industrial Engineering, University of Thessaly, Pedion Areos, Volos, 38334, Greece

Received 16 June 2007; received in revised form 12 September 2007; accepted 14 October 2007

Available online 24 October 2007

Abstract

The fully developed flow of rarefied gases through circular ducts of concentric annular cross sections is solved via kinetic theory. The flow is due to an externally imposed pressure gradient in the longitudinal direction and it is simulated by the BGK kinetic equation, subject to Maxwell diffuse-specular boundary conditions. The approximate principal of the hydraulic diameter is investigated for first time in the field of rarefied gas dynamics. For the specific flow pattern, in addition to the flow rates, results are reported for the Poiseuille number and the exact hydraulic diameter. The corresponding parameters include the whole range of the Knudsen number and various values of the accommodation coefficient and the ratio of the inner over the outer radius. The accuracy of the results is validated in several ways, including the recovery of the analytical solutions at the hydrodynamic and free molecular limits.

Keywords: Kinetic theory; Rarefied gases; Knudsen number; Microflows; Vacuum flows

1. Introduction

During the last decade, research in rarefied gas dynamics has attracted a lot of attention. This refreshed interest is due to applications in the emerging field of nano- and micro-fluidics, as well as to the more traditional fields of vacuum technology under low, medium and high vacuum conditions and high altitude aerodynamics. In addition, nowadays, due to the availability of high speed parallel computers and due to the significant advancement in computational kinetic theory made during the last years it is possible by implementing kinetic type algorithms to solve in a computationally efficient manner multidimensional problems in complex geometries.

A very common and basic rarefied flow is the fully developed flow through long channels of various cross sections. When the flow is slightly rarefied (not far from local equilibrium) as is the case in the so-called slip regime, it may be simulated by the Navier–Stokes equations subject to first and second order slip boundary conditions [1,2]. In this case, analytical solutions are plausible for channels of various cross sections including circular, annular circular, orthogonal and equilateral triangular shapes [3–8]. For channels with other cross sections, when an analytical solution is not possible, numerical solutions may be obtained with small computational effort [9]. It is noted that in several of

* Corresponding author.
E-mail address: diva@mie.uth.gr (D. Valougeorgis).

0997-7546/$ – see front matter
doi:10.1016/j.euromechflu.2007.10.002

the cited papers [6–9] the implemented slip boundary conditions are not properly defined. A complete and rigorous definition of the slip boundary conditions and the associated coefficients may be found in [2,10]. In any case, it is evident that such an approach, based on the Navier–Stokes equations, is valid only in the slip regime and collapses as the Knudsen number is increased and we depart far enough from local equilibrium, where the Newton–Fourier constitutive laws do not hold any more.

Flows far from local equilibrium (moderate or highly rarefied) can be simulated by using kinetic theory [11,12]. In particular, it has been pointed out that fully developed (linear) non-equilibrium gas flows can be handled in a very efficient manner by implementing linearized kinetic models, which over the years have been well developed in the field of rarefied gas dynamics [3,10]. The main advantage of the kinetic approach is that the solution is valid in the whole range of the Knudsen number from the free molecular, through the transition and slip regimes all the way up to the hydrodynamic limit. Therefore, non-equilibrium transport phenomena, which appear as we depart from the continuum limit, can be investigated in a thorough and systematic manner following a unified methodology without resorting to the implementation of hybrid schemes. Fully developed flows of single gases through ducts of various cross sections due to pressure and temperature gradients have been solved very accurately by applying suitable kinetic models for isothermal and non-isothermal flows respectively [13,14,16,4,15,5,17,18]. This work has been extended to binary gas mixtures by solving two coupled linearized Boltzmann equations [19–22]. The results are accurate in the whole range of the Knudsen number and they are obtained with modest computational effort, which in any case is considerably less than the one required with the DSMC method. All these efforts, clearly indicate, that kinetic solutions are capable of solving not only idealized one-dimensional flows, such as the classical one-dimensional Poiseuille, Couette and thermal creep flows, but also two and possibly three-dimensional flows, which commonly appear in technological applications.

An issue of practical interest in internal flows is the concept of the hydraulic diameter, which has been extensively used in classical hydrodynamics [23]. It is well known that this valuable principal is not exact and the introduced error depends on the cross section of the non-circular channel. At the continuum limit the discrepancy of the approximate compared to the exact hydraulic diameter has been studied in detail [23–25]. No such effort, has been reported so far in the field of internal rarefied gas flows.

In this context, the present work is devoted to the kinetic solution of the flow of a rarefied gas through circular ducts of concentric annular cross sections. The flow is due to a pressure gradient imposed in the longitudinal direction. This flow configuration has been solved by using the integro-moment method in an early work [26], where results are provided only for the flow rates with purely diffuse reflection. Here, the Maxwell diffuse-specular boundary conditions are implemented and results are provided for three values of the accommodation coefficient. More important, the Poiseuille number defined as the product of the Darcy friction factor times the Reynolds number is estimated for this particular flow configuration in the whole range of gas rarefaction. Even more, a study on the concept of the hydraulic diameter in rarefied gas dynamics is performed. In particular, the approximation, which is introduced by the implementation of the hydraulic diameter for non-circular pipes is investigated in the whole range of gas rarefaction. An expression for the estimation of the exact hydraulic diameter, which can be applied to any cross section, is derived and based on this formula, results for the exact hydraulic diameter for the concentric annulus flow are provided.

2. Flow configuration

Consider the non-equilibrium flow of a gas through a long tube of length L with constant concentric circular annular cross section connecting two vessels maintained at pressures P_1 and P_2, with $P_1 > P_2$. The annular cross section is defined by two concentric cycles of radius R_1 and R_2, with $R_1 \leqslant r' \leqslant R_2$. The perimeter and the area of the cross section are defined by $\Gamma' = 2\pi(R_1 + R_2)$ and $A' = \pi(R_2^2 - R_1^2)$ respectively, while the hydraulic diameter of the annulus, defined by

$$D_h = \frac{4A'}{\Gamma'} = 2(R_2 - R_1), \tag{1}$$

is taken as the characteristic macroscopic length of the problem. The flow is considered as fully developed in the longitudinal direction z' ($D_h \ll L$) and end effects in that direction are neglected. Therefore, the only nonzero component of the macroscopic velocity is the one in the z' direction and it is denoted by $u'(r')$. Another macroscopic distribution of practical interest is the shear stress $\tau'(r')$.

The main flow parameter is the Knudsen number. However, for purposes related to the more comprehensive presentation of the results, the so-called rarefaction parameter, defined as

$$\delta = \frac{D_h P}{\mu_0 v_0} = \frac{\sqrt{\pi}}{2}\frac{1}{Kn} \tag{2}$$

is used. Here, in addition to the hydraulic diameter D_h, which is the characteristic macroscopic length, $P = (P_1 + P_2)/2$ is a reference pressure, μ_0 is the gas viscosity at reference temperature T_0 and $v_0 = \sqrt{2RT_0}$ is the characteristic molecular velocity, with $R = k/m$ denoting the gas constant (k is the Boltzmann constant and m the molecular mass). As it is seen the rarefaction parameter is defined in terms of measurable quantities and it is proportional to the inverse Knudsen number.

It is convenient to introduce the non-dimensional spatial variables $r = r'/D_h$ and $z = z'/D_h$. Then, $r_1 \leqslant r \leqslant r_2$, where $r_1 = R_1/D_h$ and $r_2 = R_2/D_h$. In addition, we define the dimensionless cross section $A = A'/D_h^2$ and perimeter $\Gamma = \Gamma'/D_h$, while $A/\Gamma = 1/4$. The macroscopic distributions of the velocity $u'(r')$ and the shear stress $\tau'(r')$, are non-dimensionalized as $u = u'/(v_0 X_P)$ and $\tau = \tau'/(2PX_P)$ respectively, where

$$X_P = \frac{D_h}{P}\frac{dP}{dz'} = \frac{1}{P}\frac{dP}{dz} \tag{3}$$

is the dimensionless local pressure gradient causing the flow.

3. Kinetic equations, boundary conditions and solution

We implement the linearized BGK equation, which has been shown to provide reliable results in the case of isothermal flows, subject to Maxwell diffuse-specular boundary conditions. The combination of diffuse and specular reflection at the wall pertains to the surface characterization and thus to a more consistent and reliable comparison with experimental results.

Since a kinetic approach is followed, the main unknown is the distribution function, which, in general, for steady-state problems is a function of six independent variables. Here, since the flow is fully developed and axisymmetric the number of variables is reduced down to three and the main unknown is the so-called reduced distribution function $\phi = \phi(r, \zeta, \theta)$, where r is the spatial variable, while $0 \leqslant \zeta < \infty$ and $0 \leqslant \theta \leqslant 2\pi$ are the magnitude and the polar angle respectively, of the two-component dimensionless molecular velocity vector $\mathbf{c} = (\zeta, \theta)$.

The flow may be simulated by the linearized reduced BGK kinetic equation given by

$$\zeta\left[\cos\theta\frac{\partial\phi}{\partial r} - \frac{\sin\theta}{r}\frac{\partial\phi}{\partial\theta}\right] + \delta\phi = \delta u - \frac{1}{2}, \tag{4}$$

with $r_1 \leqslant r \leqslant r_2$, while the macroscopic velocity at the right-hand side is

$$u(r) = \frac{1}{\pi}\int_0^{2\pi}\int_0^{\infty} \phi\zeta e^{-\zeta^2}\, d\zeta\, d\theta. \tag{5}$$

At the inner and outer boundaries the gas–surface interaction is modeled as

$$\phi^{(+)} = (1-\alpha)\phi^{(-)}, \qquad \mathbf{c}\cdot\mathbf{n} > 0. \tag{6}$$

The superscripts $(+)$ and $(-)$ denote distributions leaving from and arriving to the boundaries respectively, while $\mathbf{n}$ is the unit vector normal to the boundaries and pointing towards the flow. The coefficient $0 \leqslant \alpha \leqslant 1$ is the momentum accommodation coefficient and corresponds to the percentage of diffuse reflection of the gas at the wall. In addition, the shear stress is computed by

$$\tau(r) = \frac{1}{\pi}\int_0^{2\pi}\int_0^{\infty} \phi\zeta^2\cos\theta\, e^{-\zeta^2}\, d\zeta\, d\theta. \tag{7}$$

The linear integro-differential problem defined by Eqs. (4) and (5), with the boundary condition (6) is discretized and then it is solved in an iterative manner. The discretization is performed in the molecular velocity and physical

spaces. Since the solution methodology has been repeatedly described and applied in previous work [15,4,21] solving flows through channels of circular and rectangular cross sections, here, for completeness, we present briefly only the main issues.

In the molecular velocity space the discretization is performed by the discrete velocity method [21], where the continuum spectrum (ζ, θ) is replaced by a suitable set of discrete velocities (ζ_m, θ_n), defined by $0 \leqslant \zeta_m < \infty$ and $0 \leqslant \theta_n \leqslant 2\pi$, with $m = 1, 2, \ldots, M$ and $n = 1, 2, \ldots, N$. We choose ζ_m to be the roots of the Legendre polynomials of order M, while $\theta_n = n\Delta\theta$, with $\Delta\theta = 2\pi/N$. The resulting set is consisting of $M \times N$ discrete velocities. In the physical space the distance $r_1 \leqslant r \leqslant r_2$ is divided in equal intervals and the discretization at each interval $i = 1, 2, \ldots, I$ is performed by the diamond-difference scheme. This is a second order central finite difference scheme, which has been extensively used in solving elliptic type linear integro-differential equations [27,21].

Applying the above discretization to Eq. (4) we deduce its discretized version

$$\begin{aligned}
&\left[\frac{\zeta_m\cos(\theta_n)}{2\Delta r} - \frac{\zeta_m\sin(\theta_n)}{(r_{i+1}+r_i)\Delta\theta} + \frac{\delta}{4}\right]\phi^{(k+1/2)}_{i+1,m,n+1} + \left[\frac{\zeta_m\cos(\theta_n)}{2\Delta r} + \frac{\zeta_m\sin(\theta_n)}{(r_{i+1}+r_i)\Delta\theta} + \frac{\delta}{4}\right]\phi^{(k+1/2)}_{i+1,m,n} \\
&\quad + \left[-\frac{\zeta_m\cos(\theta_n)}{2\Delta r} - \frac{\zeta_m\sin(\theta_n)}{(r_{i+1}+r_i)\Delta\theta} + \frac{\delta}{4}\right]\phi^{(k+1/2)}_{i,m,n+1} + \left[-\frac{\zeta_m\cos(\theta_n)}{2\Delta r} + \frac{\zeta_m\sin(\theta_n)}{(r_{i+1}+r_i)\Delta\theta} + \frac{\delta}{4}\right]\phi^{(k+1/2)}_{i,m,n} \\
&\quad = \delta\frac{u^{(k)}_{i+1} + u^{(k)}_i}{2} - \frac{1}{2},
\end{aligned} \tag{8}$$

where $\phi(r_i, \zeta_m, \theta_n) = \phi_{i,m,n}$, while the macroscopic velocity at each node of the physical grid, appearing at the right-hand side of these equations is estimated by the double summation

$$u^{(k+1)}_i = \frac{1}{\pi}\sum_m\sum_n w_m w_n \phi^{(k+1/2)}_{i,m,n}. \tag{9}$$

The Gauss–Legendre quadrature is used in the ζ variable and the trapezoidal rule in the θ variable, while w_m and w_n are the corresponding weighting factors. The shear stress $\tau(r)$, defined by Eq. (7), is estimated by applying the same quadrature.

As it has been pointed out, the whole problem is solved in an iterative manner, indicated by the superscript (k), between the kinetic equations and the integral expressions for the macroscopic quantities. It is important to note that at each iteration (k) the system of algebraic equations (8) is solved by a marching scheme and no matrix inversion is required. For each discrete velocity (ζ_m, θ_n) the distribution functions at each node are computed explicitly marching through the physical domain. The macroscopic quantity, at each physical node is computed by numerical integration using Eq. (9). The iterative procedure is ended when the imposed termination criteria on the convergence of u_i is satisfied. Following the above procedure, supplemented by a reasonable dense grid and an adequate large set of discrete velocities we are able to obtain grid independent results with modest computational effort.

4. Overall macroscopic quantities of practical interest

The kinetic solution described in the previous section yields the dimensionless macroscopic distributions of velocity and shear stress given by Eqs. (5) and (7) respectively. This solution depends on three parameters, namely the rarefaction parameter δ, the ratio R_1/R_2 and the accommodation coefficient α. Based on these results, which are valid from the free molecular, through the transition and slip regimes up to the hydrodynamic limit, several overall macroscopic quantities of practical interest may be deduced.

The mass flow rate through the concentric annulus is

$$\dot{M} = \iint_{A'} \rho u' \, dA', \tag{10}$$

where the area of the cross section A' and the macroscopic velocity u' have been defined earlier, while ρ is the local mass density. The double integral at the right-hand side of Eq. (10) is non-dimensionalized and by using the equation of state $P = \rho R T_0 = \frac{1}{2}\rho v_0^2$ we find

$$\dot{M} = G\frac{A' P X_P}{v_0} = G\frac{A' D_h}{v_0}\frac{dp}{dz'}, \tag{11}$$

where G is the non-dimensional flow rate defined by

$$G = \frac{4}{r_2^2 - r_1^2} \int_{r_1}^{r_2} u(r) r \, dr. \tag{12}$$

In a similar manner it is readily deduced that the dimensionless mean velocity is estimated by

$$\bar{u} = \frac{\overline{u'}}{v_0 X_P} = \frac{2}{r_2^2 - r_1^2} \int_{r_1}^{r_2} u(r) r \, dr. \tag{13}$$

It is seen that $G = 2\bar{u}$ and both quantities are obtained directly from the dimensionless kinetic solution.

In the case of a specific application the detailed geometry of the concentric annular tube (R_1, R_2, L) is given. In addition, the upstream and downstream pressures P_1 and P_2 respectively as well as the reference temperature T_0 are provided. Also the type of the gas and its characteristic molecular velocity v_0 are known. Then, the rarefaction parameter δ is estimated by Eq. (2) and the corresponding value of G is found by solving the kinetic equation. Finally, the mass flow rate can be estimated by the expression

$$\dot{M} = G \frac{A' D_h}{v_0} \frac{P_2 - P_1}{L}. \tag{14}$$

Eq. (14), is valid when the pressure drop is small.

Since the flow is fully developed and there is no net momentum flux in the z' direction, the net pressure and the wall shear stress are equated to yield the mean wall shear stress [23]

$$\overline{\tau'_w} = \frac{A'}{\Gamma'} \frac{dP'}{dz'}. \tag{15}$$

By non-dimensionalizing Eq. (15) it is easily deduced that the dimensionless mean wall shear stress

$$\overline{\tau_w} = \frac{\overline{\tau'_w}}{2 P X_P} = \frac{A}{2\Gamma} = \frac{1}{8}. \tag{16}$$

This result, since it is obtained by applying basic principals, is always valid independently of the rarefaction parameter δ, the ratio R_1/R_2 and the accommodation coefficient α and therefore it is used as a benchmark to test the accuracy of the kinetic calculations. This is achieved by computing the dimensionless mean wall shear stress from the kinetic solution according to

$$\overline{\tau_w} = \frac{1}{r_1 + r_2} \big[r_1 \tau(r_1) + r_2 \tau(r_2) \big], \tag{17}$$

where the quantities $\tau(r_1)$ and $\tau(r_2)$ are the shear stresses, given by Eq. (7) at the boundaries r_1 and r_2 respectively, and comparing the result of Eq. (17) with that of Eq. (16).

Another important quantity in the investigation of internal fully developed flows is the Poiseuille number Po, which is commonly defined as the product of the Darcy friction factor [23]

$$f = \frac{8 \overline{\tau'_w}}{\rho \overline{u'^2}} \tag{18}$$

times the Reynolds number

$$Re = \frac{\rho \overline{u'} D_h}{\mu}, \tag{19}$$

of the flow. Based on the implemented non-dimensionalization it is readily reduced that

$$Po = f \times Re = \frac{2\delta}{\bar{u}}. \tag{20}$$

It is seen that once the kinetic solution is obtained the Poiseuille number of the flow is easily estimated in the whole range of rarefaction.

Before we conclude this section it is noted that when the pressure difference between the upstream and downstream pressures is large, then the analysis for finding the mass flow rate $\dot{M}$ (Eq. (14)) is slightly modified. In particular, it is supplemented by a well known procedure, which is based on the mass conservation principal. In this case the mass flow rate is estimated by [3,15]

$$\dot{M} = G^* \frac{A' D_h}{v_0} \frac{P_2 - P_1}{L}, \tag{21}$$

where now G^* is an average non-dimensional flow rate defined by

$$G^* = \frac{1}{\delta_2 - \delta_1} \int_{\delta_1}^{\delta_2} G(\delta)\, d\delta, \tag{22}$$

while δ_1 and δ_2 correspond to pressures P_1 and P_2 respectively. In the case of small pressure drops we have $G^* = G$.

5. Estimation of the exact hydraulic diameter in the whole range of gas rarefaction

The concept of the hydraulic diameter is well known and widely applied in the field of continuum fluid dynamics [23]. It has been shown, based on basic principals, that the friction factor of a non-circular duct is approximately equal to the friction factor of a circular tube having diameter $D_h = 4A'/\Gamma'$. Of course, this is only an approximation since the mean velocity of the non-circular duct will not be, in general, equal to the corresponding quantity of the circular tube with diameter D_h. Following a specific procedure [23,24] the exact hydraulic diameter D_h^{exact} for which the above argument is true may be specified. It is noted that the physical meaning of the quantities D_h^{exact} (used in [23] and in the present work) and the so-called "laminar equivalent diameter" in [24] is identical. The procedure is straightforward and it is based on the estimation of the solution in the non-circular channel. At the hydrodynamic limit ($\delta \to \infty$), the departure between the exact and the approximate hydraulic diameters have been reported for several fully developed flows through ducts of various cross sections using the corresponding well known analytical solutions [23].

Now, we extend this procedure of the estimation of the exact hydraulic diameter in the field of internal rarefied gas flows. We define by Po_{tube} the Poiseuille number of a rarefied gas flow through a circular tube, while Po may be the Poiseuille number corresponding to any cross section, including the annulus one investigated in the present work. The Poiseuille numbers are estimated by Eq. (20), provided that the corresponding dimensionless mean velocity has been computed. To find the exact hydraulic diameter we write

$$f = \frac{8\overline{\tau_w'}}{\rho \overline{u'}^2} = \frac{Po_{\text{tube}}}{Re_{D_h^{\text{exact}}}}, \tag{23}$$

where

$$Re_{D_h^{\text{exact}}} = \frac{\rho \overline{u'} D_h^{\text{exact}}}{\mu} \tag{24}$$

and then solving Eq. (23) for the exact hydraulic diameter we obtain

$$D_h^{\text{exact}} = \frac{\mu \overline{u'}}{8\overline{\tau_w'}} Po_{\text{tube}}. \tag{25}$$

Eq. (25) is non-dimensionalized and the definitions of δ and Po, given by Eqs. (2) and (20) respectively, are implemented to deduce that

$$\frac{D_h^{\text{exact}}}{D_h} = \sqrt{\frac{Po_{\text{tube}}}{Po}}. \tag{26}$$

This result is quite simple, general and valid in the whole range of δ for ducts of any cross section. Using Eq. (26) it is possible to study the error which is introduced when the hydraulic diameter concept is used to approximate flows through non-circular ducts. This issue, is more valuable in the case of rarefied (non-equilibrium) flows compared to

the case of continuum (equilibrium) flows, since in the former one the required computational effort and complexity to obtain reliable results is significantly increased and therefore it is more tractable to use the hydraulic diameter concept in technological applications. In the present work the dependency of the hydraulic diameter approximation on the rarefaction parameter δ is investigated for flow through a concentric annulus and results for the exact hydraulic diameter are given in Section 7.

6. Slip regime and hydrodynamic limit

When the flow is close to local equilibrium or otherwise in the slip regime it can be simulated by the hydrodynamic equations subject to slip boundary conditions. For the particular problem under consideration the hydrodynamic equations are reduced to the Poisson equation

$$\frac{1}{r}\frac{d}{dr}\left[r\frac{du}{dr}\right] = -\delta, \quad \text{with } r_1 \leqslant r \leqslant r_2, \tag{27}$$

to be solved for the dimensionless velocity distribution $u(r)$, subject to the boundary conditions

$$u(r_1) = \frac{\sigma_P}{\delta}\frac{du}{dr}\bigg|_{r=r_1} \quad \text{and} \quad u(r_2) = -\frac{\sigma_P}{\delta}\frac{du}{dr}\bigg|_{r=r_2}, \tag{28}$$

where σ_P is the viscous slip coefficient (VSC) and it is obtained via kinetic theory by solving the so called Kramers problem. It has been found that using the BGK equation, with $\alpha = 1$ (purely diffuse scattering), we obtain $\sigma_P = 1.016$ [28], while the dependency on the accommodation coefficient can be encountered by using the expression [29,3]

$$\sigma_P(\alpha) = \frac{2-\alpha}{\alpha}\big[\sigma_P(1) - 0.1211(1-\alpha)\big]. \tag{29}$$

The corresponding results of σ_P, based on the Boltzmann equation or other kinetic model equations, are very close to the ones obtained by the BGK model [30,31].

Solving Eq. (27), with the boundary conditions given by Eq. (28) yields for the velocity profile

$$\begin{aligned} u(r) = {} & \frac{\delta}{4}\left[r_2^2 - r^2 - \frac{(r_1+r_2)}{2}\frac{\ln(r/r_2)}{\ln(r_1/r_2)}\right] \\ & + \sigma_P\left[\frac{\ln(r_1/r)[-{r_1}^3 + r_1{r_2}^2 + 2r_1{r_2}^2\ln(r_1/r_2)] + [-{r_1}^2r_2 + {r_2}^3 + 2{r_1}^2r_2\ln(r_1/r_2)]\ln(r_2/r)}{4r_1r_2[\ln(r_1/r_2)]^2}\right], \end{aligned} \tag{30}$$

where $r_1 = R_1/D_h$ and $r_2 = R_2/D_h$. Then, integrating the velocity profile (30) according to Eq. (12) the dimensionless flow rate is found to be

$$\begin{aligned} G &= G_h + G_s \\ &= \frac{\delta}{4}\left[{r_1}^2 + {r_2}^2 + \frac{1}{2}\frac{r_1+r_2}{\ln(r_1/r_2)}\right] + \sigma_P\left[\frac{1}{2} + 2r_1r_2 + \frac{r_1+r_2}{\ln(r_1/r_2)} + \frac{(r_1+r_2)^2}{8r_1r_2[\ln(r_1/r_2)]^2}\right]. \end{aligned} \tag{31}$$

At the right-hand side of Eqs. (30) and (31), the first terms correspond to the hydrodynamic solution, which as it is seen is proportional to δ and the second ones to the slip correction. Eqs. (30) and (31) take this specific form by keeping terms up to zero order in terms of δ and neglecting terms of order $1/\delta$. In principal, this solution is valid only in the slip regime ($\delta > 10$) but due to its simplicity it may be used, to some extend, in the transition regime to provide rough estimates for practical applications.

7. Results and discussion

Results for the dimensionless flow rate G, the Poiseuille number Po and the exact hydraulic diameter D_h^{exact} are provided for the flow of a rarefied gas through a concentric annulus in the whole range of the rarefaction parameter δ, for three values of the accommodation coefficient α and with the ratio of the inner over the outer radius taking several values between zero and one ($0 \leqslant R_1/R_2 < 1$).

Depending upon the values of δ, R_1/R_2 and α the number of nodes I, M and N in the phase space has been progressively increased to ensure grid independent results up to several significant figures. In general, in rarefied

Table 1
Dimensionless flow rate G in terms of δ and R_1/R_2 with $\alpha = 1$

δ	R_1/R_2									
	0.0	0.1	0.2	0.3	0.4	0.5	0.6	0.7	0.8	0.9
0.000	0.7522	0.7711	0.7919	0.8148	0.8402	0.8695	0.9043	0.9480	1.008	1.109
0.001	0.7508	0.7695	0.7903	0.8129	0.8382	0.8673	0.9018	0.9451	1.005	1.104
0.01	0.7436	0.7617	0.7818	0.8037	0.8281	0.8560	0.8891	0.9301	0.9861	1.078
0.1	0.7152	0.7309	0.7483	0.7670	0.7876	0.8107	0.8375	0.8698	0.9118	0.9748
0.3	0.6948	0.7083	0.7229	0.7385	0.7553	0.7738	0.7945	0.8185	0.8478	0.8867
0.5	0.6887	0.7000	0.7127	0.7263	0.7408	0.7564	0.7736	0.7928	0.8151	0.8422
0.7	0.6884	0.6986	0.7099	0.7219	0.7346	0.7453	0.7626	0.7784	0.7960	0.8158
0.8	0.6894	0.6989	0.7095	0.7208	0.7327	0.7454	0.7588	0.7732	0.7889	0.8061
0.9	0.6911	0.6999	0.7098	0.7205	0.7317	0.7434	0.7559	0.7691	0.7832	0.7981
1	0.6933	0.7007	0.7101	0.7202	0.7307	0.7417	0.7533	0.7654	0.7782	0.7912
1.2	0.6987	0.7053	0.7135	0.7223	0.7316	0.7411	0.7511	0.7613	0.7717	0.7817
1.4	0.7052	0.7104	0.7174	0.7252	0.7333	0.7416	0.7502	0.7588	0.7673	0.7752
1.6	0.7126	0.7163	0.7222	0.7289	0.7359	0.7432	0.7505	0.7578	0.7648	0.7710
1.8	0.7206	0.7228	0.7276	0.7333	0.7394	0.7456	0.7519	0.7580	0.7638	0.7686
2	0.7288	0.7291	0.7329	0.7377	0.7429	0.7483	0.7537	0.7588	0.7636	0.7675
3	0.7766	0.7690	0.7674	0.7677	0.7689	0.7705	0.7723	0.7740	0.7755	0.7765
5	0.8835	0.8553	0.8434	0.8365	0.8322	0.8293	0.8274	0.8261	0.8252	0.8247
10	1.174	1.082	1.047	1.027	1.015	1.007	1.002	0.9988	0.9967	0.9956
20	1.782	1.530	1.462	1.430	1.411	1.400	1.393	1.388	1.386	1.385
50	3.643	2.860	2.738	2.683	2.653	2.635	2.624	2.617	2.614	2.612
100	6.763	5.085	4.891	4.803	4.754	4.725	4.707	4.696	4.689	4.686

atmospheres (small δ) we need a large number of discrete velocities $M \times N$, while the physical grid may be coarse. From the other hand, in continuum atmospheres (large δ) the required number of discrete velocities may be reduced, but a large number of nodes I in the physical grid is important to achieve good accuracy. Indicatively, the results presented for $\delta = 1$ and for all R_1/R_2 have been obtained with $I = 500$, $M = 64$ and $N = 400$, while a further refinement of the grid does not change the results up to at least three significant figures. The number of iterations required for convergence is increased as δ is increased. In particular, with a relative convergence criterion of 10^{-7}, the number of required iterations for $\delta = 1$, 10 and 10^2 is 34, 208 and 5842 respectively. A detailed study on the convergence issues of the numerical algorithm is presented in [17]. The computational time aspect of the calculations can be regarded as modest ranging from a few seconds to a few hours as δ increases on a single core $\times 86 - 64$ CPU.

In addition to grid refinement the validation of the results has been also confirmed in the following ways. For each set of parameters, the dimensionless mean wall shear stress is computed by the kinetic algorithm and in all cases, the analytical result for the same quantity, given by Eq. (16), is obtained. Also the results have been successfully compared with the corresponding analytical ones at the free molecular and continuum limits. In particular, at large values of δ, there is very good agreement between the kinetic results and the ones based on the analytical slip solution, given by Eq. (31). Also, at $\delta = 0$, there is excellent agreement with the corresponding analytical results based on the closed form expression, given in [26]. Based on the above, the kinetic solution is considered accurate up to at least three significant figures.

Tabulated results of the dimensionless flow rate G in terms of δ and R_1/R_2, with $\alpha = 1$, 0.85 and 0.7, are given in Tables 1, 2 and 3 respectively. These specific values of α represent a wide range of gases and surfaces since in most experimentally observed cases $0.6 < \alpha \leqslant 1$ [32,33]. Results for the case of a tube ($R_1/R_2 = 0$) are also included for completeness and comparison purposes. The discrepancy of these results (second column in Tables 2, 3 and 4) with the ones published in [3] is due to the applied discretization, which here is based on the hydraulic diameter and not on the radius of the tube as it is commonly done. However, the present discretization is crucial for the purposes of the present work.

It is seen in Tables 1, 2 and 3 that, for each value of R_1/R_2 the dependency of G in terms of δ is qualitatively similar to the one for the classical case of $R_1/R_2 = 0$. It may be interested to note that as the ratio R_1/R_2 is increased the Knudsen minimum is observed at larger values of δ. The same trend on the Knudsen minimum is observed as α

Table 2
Dimensionless flow rate G in terms of δ and R_1/R_2 with $\alpha = 0.85$

δ	R_1/R_2									
	0.0	0.1	0.2	0.3	0.4	0.5	0.6	0.7	0.8	0.9
0.000	1.018	1.043	1.071	1.102	1.136	1.176	1.223	1.282	1.363	1.499
0.001	1.015	1.039	1.067	1.098	1.132	1.171	1.217	1.276	1.355	1.488
0.01	0.9993	1.023	1.049	1.079	1.111	1.148	1.191	1.245	1.318	1.437
0.1	0.9406	0.9596	0.9813	1.005	1.030	1.058	1.091	1.130	1.179	1.252
0.3	0.8961	0.9118	0.9289	0.9470	0.9664	0.9876	1.011	1.038	1.069	1.110
0.5	0.8787	0.8909	0.9054	0.9207	0.9368	0.9540	0.9726	0.9931	1.016	1.043
0.7	0.8715	0.8824	0.8948	0.9079	0.9216	0.9360	0.9513	0.9677	0.9854	1.005
0.8	0.8700	0.8800	0.8915	0.9036	0.9164	0.9297	0.9437	0.9584	0.9741	0.9907
0.9	0.8695	0.8786	0.8893	0.9006	0.9124	0.9247	0.9375	0.9509	0.9649	0.9792
1	0.8699	0.8771	0.8871	0.8977	0.9088	0.9202	0.9320	0.9442	0.9567	0.9693
1.2	0.8724	0.8789	0.8873	0.8964	0.9059	0.9156	0.9256	0.9357	0.9458	0.9553
1.4	0.8767	0.8815	0.8886	0.8964	0.9046	0.9129	0.9214	0.9298	0.9380	0.9454
1.6	0.8824	0.8855	0.8913	0.8979	0.9048	0.9120	0.9191	0.9262	0.9328	0.9386
1.8	0.8890	0.8905	0.8950	0.9005	0.9064	0.9124	0.9184	0.9243	0.9297	0.9342
2	0.8964	0.8953	0.8986	0.9031	0.9081	0.9133	0.9184	0.9239	0.9278	0.9315
3	0.9408	0.9320	0.9295	0.9291	0.9298	0.9311	0.9325	0.9339	0.9351	0.9359
5	1.046	1.016	1.003	0.9954	0.9905	0.9872	0.9849	0.9834	0.9824	0.9818
10	1.337	1.245	1.208	1.188	1.175	1.166	1.161	1.157	1.155	1.154
20	1.946	1.699	1.629	1.594	1.574	1.562	1.555	1.550	1.547	1.546
50	3.809	3.040	2.910	2.852	2.820	2.801	2.789	2.782	2.778	2.776
100	6.930	5.271	5.067	4.975	4.923	4.893	4.874	4.862	4.855	4.852

Table 3
Dimensionless flow rate G in terms of δ and R_1/R_2 with $\alpha = 0.7$

δ	R_1/R_2									
	0.0	0.1	0.2	0.3	0.4	0.5	0.6	0.7	0.8	0.9
0.000	1.397	1.430	1.469	1.511	1.559	1.613	1.677	1.758	1.869	2.055
0.001	1.391	1.423	1.461	1.504	1.550	1.603	1.666	1.746	1.854	2.034
0.01	1.362	1.392	1.428	1.467	1.510	1.559	1.617	1.689	1.785	1.939
0.1	1.255	1.278	1.305	1.334	1.366	1.401	1.441	1.488	1.546	1.629
0.3	1.176	1.194	1.214	1.236	1.258	1.283	1.309	1.339	1.373	1.415
0.5	1.144	1.156	1.173	1.190	1.208	1.227	1.247	1.269	1.293	1.320
0.7	1.127	1.139	1.153	1.167	1.181	1.197	1.213	1.230	1.247	1.266
0.8	1.123	1.133	1.145	1.159	1.172	1.186	1.200	1.216	1.231	1.247
0.9	1.120	1.129	1.140	1.152	1.164	1.177	1.190	1.204	1.217	1.231
1	1.118	1.124	1.134	1.146	1.157	1.169	1.181	1.193	1.206	1.217
1.2	1.117	1.123	1.131	1.141	1.150	1.160	1.170	1.180	1.189	1.198
1.4	1.118	1.122	1.129	1.137	1.145	1.153	1.162	1.170	1.177	1.184
1.6	1.122	1.124	1.130	1.136	1.143	1.149	1.156	1.163	1.169	1.175
1.8	1.127	1.127	1.131	1.137	1.142	1.148	1.153	1.159	1.168	1.168
2	1.133	1.129	1.132	1.136	1.141	1.146	1.151	1.155	1.160	1.163
3	1.173	1.163	1.159	1.158	1.158	1.159	1.160	1.161	1.163	1.163
5	1.277	1.244	1.230	1.221	1.216	1.212	1.209	1.208	1.206	1.206
10	1.567	1.474	1.437	1.415	1.401	1.392	1.386	1.382	1.380	1.379
20	2.178	1.936	1.863	1.826	1.805	1.792	1.783	1.778	1.776	1.775
50	4.042	3.290	3.152	3.090	3.055	3.035	3.022	3.015	3.010	3.009
100	7.163	5.529	5.313	5.215	5.161	5.128	5.108	5.096	5.089	5.086

is decreased. Also, as expected, when the accommodation coefficient is decreased the dimensionless flow rate is increased.

Next, a comparison between the kinetic and slip solutions is performed. In Fig. 1, for the specific case of $R_1/R_2 = 0.5$, with $\alpha = 1.0$ and 0.7, the slip results obtained by Eq. (31) and the corresponding kinetic ones (seventh column in Tables 1 and 3) are plotted in terms of δ. It is seen that for $\delta > 10$ the agreement between the two solutions is good.

Table 4
The quantities G_h/δ and G_s/σ_P of Eq. (31) in terms R_1/R_2

	R_1/R_2									
	0.0	0.1	0.2	0.3	0.4	0.5	0.6	0.7	0.8	0.9
G_h/δ	0.0625	0.0447	0.0433	0.0426	0.0422	0.0420	0.0418	0.0417	0.0417	0.0417
G_s/σ_P	0.500	0.582	0.538	0.520	0.512	0.507	0.504	0.502	0.501	0.500

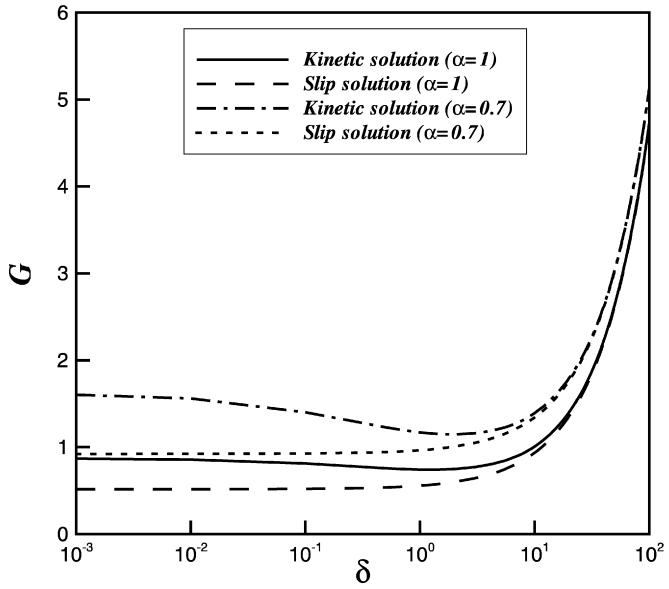

Fig. 1. Comparison of dimensionless flow rate G between the kinetic and slip (Eq. (31)) solutions in terms of δ for a concentric annulus with $R_1/R_2 = 0.5$ and $\alpha = 1.0$ and 0.7.

More precisely, by comparing the kinetic and the slip results for $\alpha = 1.0$, it is found that the relative error in the slip solution at $\delta = 2$ and 10 is 19.9% and 7.1% respectively, at $\delta = 20$ reduces to 3.2%, while at $\delta = 50$ becomes only 0.8%. Also, as α is decreased the discrepancy of the slip solution is increased but not significantly. These results are indicative for all the ratios of the inner over the outer radius R_1/R_2. We complete our discussion on the slip solution by providing, in Table 4, results for G_h/δ and G_s/σ_P, which correspond to the quantities in the two brackets at the right-hand side of Eq. (31) in terms of the ratio R_1/R_2. The results in Table 4 are helpful in order to distinguish between the hydrodynamic solution and the slip correction.

Based on the mean dimensionless bulk velocity obtained by the kinetic solution, tabulated results for the Poiseuille number of the concentric annular tube flow in terms of δ and R_1/R_2, with $\alpha = 1$, 0.85 and 0.7, are given in Tables 5, 6 and 7 respectively. The following remarks can be made. For $10^{-3} \leqslant \delta \leqslant 10^{-1}$ (free molecular regime), the *Po* number is increased directly proportional to δ. Then, for $10^{-1} < \delta < 10$ (transition regime), the *Po* number keeps increasing as δ is increased but in a slower pace. Finally, for $\delta \geqslant 10$ (slip regime), as δ is increased, the *Po* number is increased very slowly, reaching asymptotically the continuum results at the hydrodynamic limit (last raw in Tables 6, 7 and 8), which have been obtained by Eq. (31) at $\delta \to \infty$. These remarks apply to all values of the ratios of the inner over the outer radius and accommodation coefficients. Also, for the same δ, as R_1/R_2 is increased the *Po* number is also increased, while as α is decreased the *Po* number is decreased.

Using Eq. (26) and the results in Tables 5, 6 and 7, the validity of the concept of the hydraulic diameter can be checked by comparing the approximate with the exact hydraulic diameters D_h and D_h^{exact} respectively. In Fig. 2, the relative percent error in the approximate hydraulic diameter in terms of R_1/R_2 and for various values of δ, with $\alpha = 1.0$, is plotted. It is seen that at each R_1/R_2 the maximum percent error is positive and occurs at the hydrodynamic limit as $\delta \to \infty$. This specific plot ($\delta \to \infty$) is in excellent agreement with the corresponding one, presented in

Table 5
The Poiseuille number *Po* in terms of δ and R_1/R_2 with $\alpha = 1$

δ	R_1/R_2									
	0.0	0.1	0.2	0.3	0.4	0.5	0.6	0.7	0.8	0.9
0.001	0.533(−2)	0.519(−2)	0.506(−2)	0.492(−2)	0.477(−2)	0.461(−2)	0.443(−2)	0.423(−2)	0.398(−2)	0.362(−2)
0.01	0.540(−1)	0.524(−1)	0.511(−1)	0.497(−1)	0.483(−1)	0.467(−1)	0.449(−1)	0.430(−1)	0.405(−1)	0.371(−1)
0.1	0.559	0.547	0.535	0.522	0.508	0.493	0.477	0.460	0.439	0.410
0.3	1.73	1.70	1.66	1.63	1.59	1.55	1.51	1.47	1.42	1.35
0.5	2.90	2.90	2.81	2.76	2.70	2.65	2.58	2.52	2.45	2.38
1	5.77	5.71	5.63	5.56	5.47	5.39	5.31	5.23	5.14	5.06
1.5	8.46	8.42	8.35	8.26	8.17	8.09	8.00	7.92	7.83	7.76
2	11.0	11.0	10.9	10.8	10.8	10.7	10.6	10.5	10.5	10.4
3	15.5	15.6	15.6	15.6	15.6	15.6	15.5	15.5	15.5	15.5
5	22.6	23.4	23.7	23.9	24.0	24.1	24.2	24.2	24.2	24.2
10	34.1	37.0	38.2	39.0	39.4	39.7	39.9	40.0	40.1	40.2
20	44.9	52.3	54.7	55.9	56.7	57.1	57.4	57.6	57.7	57.8
50	54.9	69.9	73.1	74.5	75.4	75.9	76.2	76.4	76.5	76.6
100	59.1	78.7	81.9	83.3	84.1	84.7	85.0	85.2	85.3	85.4
200	61.5	83.8	86.9	88.4	89.2	89.7	90.1	90.3	90.4	90.5
500	63.0	87.1	90.1	91.6	92.4	93.0	93.3	93.5	93.6	93.7
1000	63.9	88.2	91.2	92.7	93.6	94.1	94.4	94.6	94.8	94.8
.										
.										
∞	64.0	89.4	92.4	93.8	94.7	95.3	95.6	95.8	95.9	96.0

Table 6
The Poiseuille number *Po* in terms of δ and R_1/R_2 with $\alpha = 0.85$

δ	R_1/R_2									
	0.0	0.1	0.2	0.3	0.4	0.5	0.6	0.7	0.8	0.9
0.001	0.394(−2)	0.385(−2)	0.375(−2)	0.364(−2)	0.353(−2)	0.341(−2)	0.328(−2)	0.313(−2)	0.295(−2)	0.269(−2)
0.01	0.400(−1)	0.391(−1)	0.381(−1)	0.370(−1)	0.360(−1)	0.348(−1)	0.335(−1)	0.321(−1)	0.303(−1)	0.278(−1)
0.1	0.425	0.417	0.408	0.398	0.388	0.378	0.367	0.354	0.339	0.319
0.3	1.34	1.32	1.29	1.27	1.24	1.22	1.19	1.16	1.12	1.08
0.5	2.28	2.25	2.21	2.17	2.13	2.10	2.06	2.01	1.97	1.92
1	4.60	4.56	4.51	4.45	4.40	4.35	4.29	4.24	4.18	4.13
1.5	6.83	6.80	6.75	6.70	6.64	6.58	6.53	6.47	6.42	6.38
2	8.93	8.94	8.90	8.86	8.81	8.76	8.72	8.67	8.62	8.58
3	12.8	12.9	12.9	12.9	12.9	12.9	12.9	12.8	12.8	12.8
5	19.1	19.7	19.9	20.1	20.2	20.3	20.3	20.3	20.4	20.4
10	29.9	32.1	33.1	33.7	34.0	34.3	34.5	34.6	34.6	34.7
20	41.1	47.1	49.1	50.2	50.8	51.2	51.4	51.6	51.7	51.7
50	52.5	65.8	68.7	70.1	70.9	71.4	71.7	71.9	72.0	72.0
100	57.7	75.9	78.9	80.4	81.3	81.7	82.1	82.3	82.4	82.4
200	60.7	82.2	85.2	86.7	87.6	88.1	88.4	88.6	88.7	88.8
500	62.3	86.3	89.4	90.8	91.7	92.2	92.6	92.8	92.9	93.0
1000	63.7	87.8	90.8	92.3	93.2	93.7	94.1	94.3	94.4	94.5
.										
.										
∞	64.0	89.4	92.4	93.8	94.7	95.3	95.6	95.8	95.9	96.0

Figs. 3–9 of the classical textbook of White [23]. As the flow departs from local equilibrium and δ is decreased the error is reduced up to $\delta \simeq 3$, where it is very close to zero. Then, as δ is further decreased the percent error becomes negative and it is increased by taking larger negative values all the way down to the free molecular region ($\delta = 10^{-3}$). It is also seen that at each δ the relative error (either positive or negative) is always increased as the ratio R_1/R_2 is increased. Both, the maximum positive and negative percent errors are observed at $R_1/R_2 = 0.9$ and for $\delta \to \infty$

Table 7
The Poiseuille number Po in terms of δ and R_1/R_2 with $\alpha = 0.7$

δ	R_1/R_2									
	0.0	0.1	0.2	0.3	0.4	0.5	0.6	0.7	0.8	0.9
0.001	0.287(−2)	0.281(−2)	0.273(−2)	0.266(−2)	0.258(−2)	0.249(−2)	0.240(−2)	0.229(−2)	0.215(−2)	0.196(−2)
0.01	0.293(−1)	0.287(−1)	0.280(−1)	0.272(−1)	0.265(−1)	0.256(−1)	0.247(−1)	0.237(−1)	0.224(−1)	0.206(−1)
0.1	0.319	0.313	0.307	0.300	0.293	0.286	0.278	0.269	0.259	0.246
0.3	1.02	1.01	0.988	0.971	0.954	0.935	0.917	0.896	0.874	0.848
0.5	1.75	1.73	1.715	1.68	1.66	1.63	1.60	1.58	1.55	1.515
1	3.58	3.56	3.53	3.49	3.46	3.42	3.39	3.35	3.32	3.287
1.5	5.36	5.35	5.32	5.29	5.25	5.22	5.18	5.15	5.12	5.089
2	7.06	7.09	7.07	7.04	7.01	6.98	6.95	6.93	6.90	6.879
3	10.2	10.3	10.4	10.4	10.4	10.4	10.3	10.3	10.3	10.3
5	15.7	16.1	16.3	16.4	16.4	16.5	16.5	16.6	16.6	16.6
10	25.5	27.1	27.8	28.3	28.6	28.7	28.9	28.9	29.0	29.0
20	36.7	41.3	42.9	43.8	44.3	44.6	44.9	45.0	45.0	45.1
50	49.5	60.8	63.5	64.7	65.5	65.9	66.2	66.3	66.4	66.5
100	55.8	72.3	75.3	76.7	77.5	78.0	78.3	78.5	78.6	78.6
200	59.7	79.9	83.0	84.5	85.3	85.8	86.2	86.4	86.8	86.5
500	62.3	85.3	88.4	89.9	90.7	91.2	91.6	91.8	91.9	92.0
1000	63.7	87.3	90.3	91.8	92.7	93.2	93.5	93.7	93.8	93.9
.										
.										
∞	64.0	89.4	92.4	93.8	94.7	95.3	95.6	95.8	95.9	96.0

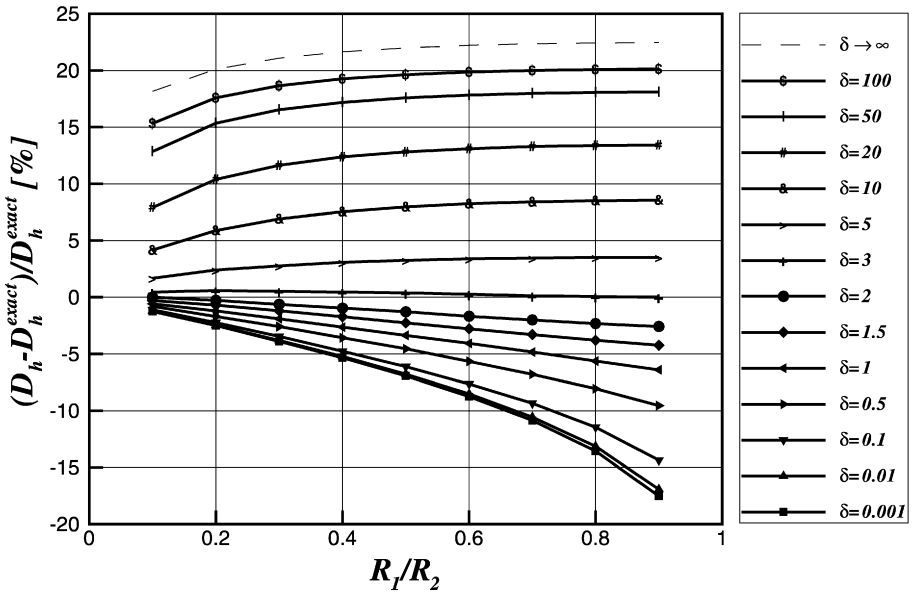

Fig. 2. Percent error in the approximate hydraulic diameter compared to the exact hydraulic diameter for concentric annular tubes, with $a = 1$ and various δ.

and $\delta = 10^{-3}$ respectively, where the corresponding estimates are $+22.5\%$ and -17.5%. Finally, it is noted that for small values of R_1/R_2 and $\delta \leqslant 5$ the percent error varies between $\pm 5\%$. Very similar behavior of the percent error in terms of δ and R_1/R_2 has been found for the cases of $\alpha = 0.85$ and 0.7. Although general conclusions cannot be easily drawn, it may be stated that for the present flow configuration in all cases tested the error introduced by the implementation of the approximate hydraulic radius is smaller in the rarefied than in the corresponding continuum flow.

8. Concluding remarks

The fully developed flow of rarefied gases in concentric annular tubes due to an imposed pressure gradient has been investigated implementing a kinetic approach. The BGK kinetic equation, associated with Maxwell diffuse-specular boundary conditions, has been solved by the discrete velocity method. Results are provided for the flow rates and the Poiseuille number for various concentric annular cross sections in the whole range of the rarefaction parameter δ and for three values of the accommodation coefficient. It has been found that in the free molecular regime ($\delta \leqslant 10^{-1}$) the Poiseuille number is increased proportionally to δ, then in the transition regime ($0.1 < \delta < 10$) it keeps increasing but in a slower pace and finally in the slip regime ($\delta \geqslant 10$) it is increased very slowly, reaching asymptotically the continuum result at the hydrodynamic limit ($\delta \to \infty$). Also, an expression for the estimation of the exact hydraulic diameter in the whole range of gas rarefaction is derived and then it is applied in the present flow configuration to yield the percent error in the approximate hydraulic diameter compared to the exact one. A detailed quantitative description of the error in terms of δ and the ratio of the inner over the outer radius is provided. In all cases tested the estimated error is smaller in the rarefied than in the corresponding continuum flow. The validity and the accuracy of the kinetic results have been verified in several ways including the recovery of the well known solutions at the hydrodynamic and free molecular limits.

The proposed methodology for the estimation of the discrepancy between the exact and approximate hydraulic diameters may be applied in a straightforward manner to channels of orthogonal, triangular and trapezoidal cross sections, which are of some interest in several technological fields including nano- and micro-fluidics and vacuum technology.

Acknowledgements

Partial support by the Association EURATOM – Hellenic Republic (program on Controlled Thermonuclear Fusion) and the Greek Ministry of Education (program Pythagoras) is highly acknowledged.

References

[1] C. Cercignani, R. Illner, M. Pulvirenti, The Mathematical Theory of Dilute Gases, Springer, New York, 1994.
[2] Y. Sone, Kinetic Theory and Fluid Mechanics, Birkhäuser, Boston, 2002.
[3] F. Sharipov, V. Seleznev, Data on internal rarefied gas flows, J. Phys. Chem. Ref. Data 27 (3) (1998) 657–706.
[4] F. Sharipov, Rarefied gas flow through a long rectangular channel, J. Vac. Sci. Technol. A 17 (5) (1999) 3062–3066.
[5] F. Sharipov, Non-isothermal gas flow through rectangular microchannels, J. Micromech. Microeng. 9 (4) (1999) 394–401.
[6] C. Aubert, S. Colin, High-order boundary conditions for gaseous flows in rectangular microducts, Microscale Thermophys. Engrg. 5 (2001) 41–54.
[7] J. Maurer, P. Tabeling, P. Joseph, H. Willaime, Second-order slip laws in microchannels for helium and nitrogen, Phys. Fluids 15 (9) (2003) 2613–2621.
[8] C.Y. Wang, Slip flow in a triangular duct – an exact solution, Z. Angew. Math. Math. Mech. 83 (9) (2003) 629–631.
[9] G.L. Morini, M. Spiga, P. Tartarini, The rarefaction effect on the friction factor of gas flow in microchannels, Superlattices and Microstructures 35 (2004) 587–599.
[10] K. Aoki, Dynamics of rarefied gas flows: Asymptotic and numerical analyses of the Boltzmann equation, AIAA 2001-0874 39th AIAA Aerospace Sciences Meeting and Exhibit, Reno, NV, 2001.
[11] J.H. Ferziger, H.G. Kaper, Mathematical Theory of Transport Processes in Gases, North-Holland Publishing Company, Amsterdam, 1972.
[12] C. Cercignani, The Boltzmann Equation and its Application, Springer, New York, 1988.
[13] D. Valougeorgis, J.R. Thomas, Exact numerical results for Poiseuille and thermal creep flow in a cylindrical tube, Phys. Fluids 29 (1986) 423–429.
[14] K. Aoki, Numerical analysis of rarefied gas flows by finite-difference method, in: E.P. Muntz, D.P. Weaver, D.H. Campbell (Eds.), in: Rarefied Gas Dynamics, vol. 118, AIAA, Washington, DC, 1989, p. 297.
[15] F. Sharipov, V.D. Seleznev, Rarefied gas flow through a long tube at any pressure ratio, J. Vac. Sci. Technol. A 12 (5) (1994) 2933–2935.
[16] F. Sharipov, Rarefied gas flow through a long tube at any temperature ratio, J. Vac. Sci. Technol. A 14 (4) (1996) 2627–2635.
[17] D. Valougeorgis, S. Naris, Acceleration schemes of the discrete velocity method: Gaseous flows in rectangular microchannels, SIAM J. Sci. Comp. 25 (2003) 534–552.
[18] S. Naris, D. Valougeorgis, Boundary driven non-equilibrium gas flow in a grooved channel via kinetic theory, Phys. Fluids 19 (6) (2007) 067103.
[19] F. Sharipov, D. Kalempa, Gaseous mixture flow through a long tube at arbitrary Knudsen number, J. Vac. Sci. Technol. A 20 (3) (2002) 814–822.

[20] S. Takata, S. Yasuda, S. Kosuge, K. Aoki, Numerical analysis of thermal-slip ans diffusion-slip flows of a binary mixture of hard-sphere molecular gases, Phys. Fluids 15 (12) (2003) 3745–3766.
[21] S. Naris, D. Valougeorgis, F. Sharipov, D. Kalempa, Discrete velocity modelling of gaseous mixture flows in MEMS, Superlattices and Microstructures 35 (3–6) (2004) 629–643.
[22] S. Naris, D. Valougeorgis, F. Sharipov, D. Kalempa, Flow of gaseous mixtures through rectangular microchannels driven by pressure, temperature and concentration gradients, Phys. Fluids 17 (10) (2005) 100607.
[23] F.M. White, Viscous Fluid Flows, McGraw-Hill, 1974.
[24] O.C. Jones Jr., An improvement in the calculation of turbulent friction in rectangular ducts, Trans. ASME J. Fluids Eng. 98 (1976) 173–181.
[25] N.T. Obot, Determination of incompressible flow friction in smooth circular and noncircular passages: A generalized approach including validation of the nearly century old hydraulic diameter concept, Trans. ASME J. Fluids Eng. 110 (1988) 431–440.
[26] P. Bassanini, C. Cercignani, F. Sernagiotto, Flow of a rarefied gas in a tube of annular section, Phys. Fluids 9 (6) (1966) 1174–1178.
[27] E.E. Lewis, W.F. Miller Jr., Computational Methods of Neutron Transport Theory, Wiley, New York, 1984.
[28] L.B. Barichello, M. Camargo, P. Rodrigues, C.E. Siewert, Unified solution to classical flow problems based on the BGK model, Z. Angew. Math. Math. Mech. 52 (2001) 517–534.
[29] S.K. Loyalka, Momentum and temperature slip coefficients with arbitrary accommodation coefficients, J. Chem. Phys. 48 (1968) 5432–5436.
[30] C.E. Siewert, F. Sharipov, Model equations in rarefied gas dynamics: Viscous slip and thermal slip coefficients, Phys. Fluids 14 (2002) 4123–4129.
[31] T. Ohwada, Y. Sone, K. Aoki, Numerical analysis of the shear and thermal creep flows of a rarefied gas over a plane wall on the basis of the linearized Boltzmann equation for hard-sphere molecules, Phys. Fluids A 1 (1989) 1588–1599.
[32] O.V. Sazhin, S.F. Borisov, F. Sharipov, Accommodation coefficient of tangential momentum on atomically clean and contaminated surfaces, J. Vac. Sci. Technol. A 19 (5) (2001) 2499–2503.
[33] F. Sharipov, Application of the Cercignani–Lampis scattering kernel to calculations of rarefied gas flows. III. Poiseuille flow and thermal creep through a long tube, Eur. J. Mech. B/Fluids 22 (2003) 145–154.